Scattered waves fuel emergent activity

Ella M. King,[1,2] Mia C. Morrell,[1] Jacqueline B. Sustiel,[1] Matthew Gronert,[1] Hayden Pastor,[1] and David G. Grier[1]
[1]*Department of Physics and Center for Soft Matter Research, New York University, New York, New York 10003, USA*
[2]*Center for Computational Biology, Flatiron Institute, New York, New York 10010, USA*

(Received 16 May 2024; accepted 15 December 2024; published 15 January 2025)

Active matter taps into external energy sources to power its own processes. Systems of passive particles ordinarily lack this capacity, but can become active if the constituent particles interact with each other nonreciprocally. By reformulating the theory of classical wave-matter interactions, we demonstrate that interactions mediated by scattered waves generally are not constrained by Newton's third law. The resulting center-of-mass forces propel clusters of scatterers, enabling them to extract energy from the wave and rendering them active. This form of activity is an emergent property of the scatterers' state of organization and can arise in any system where mobile objects scatter waves. Emergent activity flips the script on conventional active matter whose nonreciprocity emerges from its activity, and not the other way around. We combine theory, experiment, and simulation to illustrate how emergent activity arises in wave-matter composite systems and to explore the phenomenology of emergent activity in experimentally accessible models. These preliminary studies suggest that heterogeneity is a singular perturbation to the dynamics of wave-matter composite systems, and induces emergent activity under all but the most limited circumstances.

DOI: 10.1103/PhysRevResearch.7.013055

I. INTRODUCTION

Active matter harvests energy from its environment and reuses that energy for its own purposes—for example, to power its own motion [1–4]. Familiar examples include the molecular motors within cells [5], synthetic colloidal swimmers [6], bacterial swarms [7], and flocks of birds [8]. The individual entities that make up such systems are "active particles" in the sense that they independently transduce energy.

An alternative form of activity can arise when otherwise passive particles interact through nonreciprocal forces. The imbalance in these forces enables groups of particles to translate and rotate even when the individual particles have no mechanism to acquire the necessary energy. Hallmarks of this form of activity have been observed in simulations of two-component interdiffusing fluids [9], dispersions of catalytically active particles [10], and robotic metamaterials [11], all of which display transitions between passive and active states enabled by nonreciprocal interactions. These disparate systems exemplify a broad category of compositions of matter that display "emergent activity" in the sense that their activity is an emergent property of their state of organization. Whereas previous studies have focused on simulations of specialized model systems, we demonstrate that emergent activity arises ubiquitously in any context where mobile objects scatter waves. More specifically, we demonstrate, perhaps counterintuitively, that the wave-mediated interactions that bind scatterers into clusters need not be reciprocal. Figure 1 illustrates how the interplay of reciprocal and nonreciprocal wave-mediated interactions can organize independent passive scatterers into active clusters.

We develop the principle of emergent activity in Sec. II by focusing on sound and light as archetypal waves. In both cases, we derive analytic expressions for the wave-mediated interactions between dissimilar particles, and identify conditions under which the pair interaction is nonreciprocal. Experimental observations in Sec. III and simulations in Sec. IV reduce the theory to practice, illustrating how unbalanced acoustic forces give rise to emergent activity in monolayers of acoustically levitated granular matter. These studies reveal that heterogeneity in the particles' scattering properties constitutes a singular perturbation to the system's dynamics, which means that emergent activity should be a generic feature of any system composed of particles that scatter waves. We conclude in Sec. V with a discussion of the general consequences of emergent activity for self-organization in natural and synthetic many-body systems.

II. THE PRINCIPLE OF EMERGENT ACTIVITY

Active particles are self-propelled and so can move autonomously through their environment. Passive particles, by contrast, lack the ability to transduce energy on their own. They therefore relax into equilibrium configurations unless driven by external forces. Emergent activity provides a mechanism for certain configurations of passive particles to develop the capacity to move autonomously. This kind of collective self-propulsion arises in systems of passive particles that interact with each other through nonreciprocal forces.

The two-particle system depicted in Fig. 2 illustrates the physical basis for emergent activity and helps to clarify the distinction between conventional activity, simple driving, and

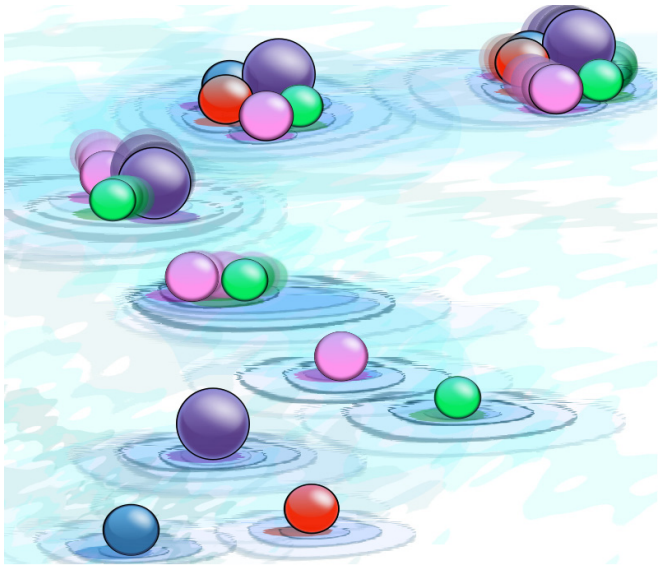

FIG. 1. Emergent activity in a wave-matter composite system. Individual particles scatter a wave symmetrically and so experience no net force. Scattered waves mediate interactions that coalesce groups of particles into pairs, trios, and larger rafts. Unless the particles have identical scattering properties, the net wave-mediated interaction transfers energy from the wave into the clusters' translational and rotational kinetic energy.

emergent activity. A passive particle located at $\boldsymbol{r}_i$ experiences a force, $\boldsymbol{F}_{ij}(\boldsymbol{r}_{ij})$, due to its interaction with its neighbor at $\boldsymbol{r}_j$. This force depends on the interparticle separation, $\boldsymbol{r}_{ij} = \boldsymbol{r}_i - \boldsymbol{r}_j$, as well as the two particles' properties. The same coupling mechanism also mediates a force, $\boldsymbol{F}_{ji}(\boldsymbol{r}_{ji})$, on particle j that is obtained from $\boldsymbol{F}_{ij}(\boldsymbol{r}_{ij})$ by exchanging the particles' labels. Newton's third law leads us to expect these forces to be reciprocal in the sense that $\boldsymbol{F}_{ij}(\boldsymbol{r}_{ij}) = -\boldsymbol{F}_{ji}(\boldsymbol{r}_{ji})$. If the interparticle interaction is nonreciprocal, however, then the net force,

$$\Delta\boldsymbol{F}_{ij}(\boldsymbol{r}_{ij}) = \boldsymbol{F}_{ij}(\boldsymbol{r}_{ij}) + \boldsymbol{F}_{ji}(\boldsymbol{r}_{ji}), \tag{1}$$

acting on the pair's center of mass need not vanish.

To show how such nonreciprocity can arise, we refer again to Fig. 2 and consider what happens when passive particles interact with an incident wave, $p_0(\boldsymbol{r}, t)$, that acts as a reservoir of energy, momentum, and angular momentum. In scattering the incident wave, each particle experiences a primary time-averaged force, $\boldsymbol{F}_i(\boldsymbol{r}_i)$, that could be used to drive its motion. Instead, we assume that the particles come to mechanical equilibrium on manifolds where $\boldsymbol{F}_i(\boldsymbol{r}_i) = 0$. In that sense, the wave does not drive the particles.

In addition to the primary force, particle i also experiences a secondary force, $\boldsymbol{F}_{ij}(\boldsymbol{r}_{ij})$, due to the wave, $p_j(\boldsymbol{r}_{ij}, t)$, that is scattered by its neighbor. Particle j experiences an analogous secondary force mediated by $p_i(\boldsymbol{r}_{ji}, t)$. In the next two sections, we formulate the time-averaged secondary interactions, $\boldsymbol{F}_{ij}(\boldsymbol{r}_{ij})$, for particles scattering either sound or light and demonstrate that those interactions are nonreciprocal unless the particles have identical scattering properties. Analytical expressions for the net center-of-mass force, $\Delta\boldsymbol{F}_{ij}(\boldsymbol{r}_{ij})$, reveal how scattering enables pairs of passive particles to propel themselves autonomously through the wave. The pair of scatterers therefore is active even though the individual particles are not.

For clarity, we focus on the time-averaged forces exerted by harmonic waves [12]. We restrict our attention to spherical particles whose scattering patterns are readily expressed as multipole expansions. We furthermore work in the Rayleigh limit, considering particles that are substantially smaller than the wavelength λ of the incident wave, and invoke the first Born approximation, limiting the analysis to first-order scattering. The interaction then is conveniently expressed in orders of the dimensionless size parameters, ka_i and ka_j, where a_i and a_j are the radii of the two spheres and $k = 2\pi/\lambda$ is the wave number. These simplifying assumptions are not required for wave-mediated interactions to display nonreciprocity. They are useful because they clarify the origin and nature of nonreciprocal interactions in model systems that lend themselves to detailed analysis.

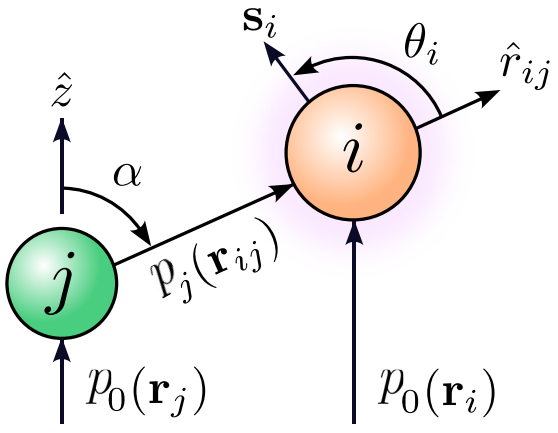

FIG. 2. Geometry for computing sound-mediated forces and interactions. Particle j scatters a portion of the incident pressure wave, $p_0(\boldsymbol{r})$, to its neighbor at $\boldsymbol{r}_i$. The scattered wave, $p_j(\boldsymbol{r}_{ij})$, contributes to the force experienced by particle i. Formulating this influence is facilitated by defining a spherical coordinate system centered on particle i and aligned with the separation between the particles, $\boldsymbol{r}_{ij} = \boldsymbol{r}_i - \boldsymbol{r}_j$.

A. Nonreciprocal interactions mediated by sound

The force landscape created by a general acoustic wave includes both nonconservative driving forces and conservative trapping forces [13]. To avoid confusion between driving and activity, we specialize to the case of a planar standing wave that exerts no driving forces. A pair of particles levitated in such a standing wave experiences a pressure field,

$$p_0(\boldsymbol{r}) = p_0 \sin(kz), \tag{2}$$

that we take to be aligned in the vertical direction $\hat{z}$. As discussed in Appendix A, a particle that is denser and less compressible than the medium experiences a primary scattering force, $\boldsymbol{F}_i(\boldsymbol{r}_i)$, that localizes it at a node of the pressure field, where the primary force vanishes. In formulating the interaction between a pair of levitated spheres, we assume that both are localized in the same nodal plane at $z = 0$. Referring to Fig. 2, this corresponds to scattering angle $\alpha = \pi/2$. The

corresponding scattering-mediated interaction between particles i and j is derived in Appendix B 2 and has the leading-order form,

$$\boldsymbol{F}^K_{ij}(\boldsymbol{r}_{ij}) = -2\pi\, F_0\, \Phi(kr_{ij})\, \eta_i \eta_j\, \hat{\boldsymbol{r}}_{ij}, \tag{3a}$$

which historically has been called the König interaction [14]. The overall scale of the König interaction is set by the intensity of the incident wave,

$$F_0 = \frac{p_0^2}{\rho_0 \omega^2}. \tag{3b}$$

Its dependence on particle separation,

$$\Phi(x) = \frac{1}{x^4}\left[\left(1 - \frac{x^2}{3}\right)\cos(x) + x\sin(x)\right], \tag{3c}$$

is shaped by the scattered wave's interference with the incident wave. The particles' properties enter into $\boldsymbol{F}^K_{ij}(\boldsymbol{r}_{ij})$ through dimensionless coupling constants of the form

$$\eta_i = \frac{\rho_0 - \rho_i}{\rho_0 + 2\rho_i}(ka_i)^3, \tag{3d}$$

each of which depends on the mismatch between the particle's density ρ_i and that of the medium ρ_0 and is proportional to the particle's volume. Equation (3) includes all contributions up to $\mathcal{O}\{(ka_i)^3(ka_j)^3\}$ in the reduced particle sizes and is reciprocal under exchange of the labels i and j. Surprisingly, the expression in Eq. (3) for the leading-order König interaction between dissimilar spheres appears not to have been reported previously.

The König interaction is attractive for small separations [15,16] and so tends to draw monolayers of levitated particles together into close-packed rafts [17–22]. The pair interaction is a central force because the two-particle system is symmetric and the wave itself carries no angular momentum [23].

Whereas the leading-order König interaction is reciprocal, the multipole expansion in Appendix B 2 reveals that next-order contributions to the interparticle force break that symmetry:

$$\boldsymbol{F}_{ij}(\boldsymbol{r}_{ij}) = \left(1 + \chi^K_{ij}\right)\boldsymbol{F}^K_{ij}(\boldsymbol{r}_{ij}), \tag{4a}$$

where the additional factor,

$$\chi^K_{ij} = \alpha_{ij} + \beta_{ij}(ka_j)^2 + \gamma_{ij}(ka_i)^2, \tag{4b}$$

includes all contributions up to $\mathcal{O}\{(ka_i)^5\}$ and $\mathcal{O}\{(ka_j)^5\}$. The coefficients of χ^K_{ij} depend on the densities and compressibilities of the two particles and are reported in Eq. (B8). These corrections to the leading-order König interaction are nonreciprocal unless the two particles have identical properties. A pair of acoustically levitated spheres therefore experiences a center-of-mass force,

$$\Delta\boldsymbol{F}^K_{ij}(\boldsymbol{r}_{ij}) = \left(\chi^K_{ij} - \chi^K_{ji}\right)\boldsymbol{F}^K_{ij}(\boldsymbol{r}_{ij}), \tag{5}$$

that the individual spheres would not have felt.

The analogous formulation of the wave-mediated pair interaction between bubbles is presented in Appendix B 3. Nonreciprocal effects tend to be much weaker for spheres that are less dense and more compressible than the medium.

B. Nonreciprocal interactions mediated by light

Pair interactions can be mediated by scattered electromagnetic waves in a phenomenon known as optical binding [24,25]. In this case, the role played by the pressure wave, $p_0(\boldsymbol{r})$, in Fig. 2 is played instead by the light's electric field, $\boldsymbol{E}_0(\boldsymbol{r})$. Transverse optical binding occurs when the interparticle separation is perpendicular to the light's axis of propagation, $\alpha = \pi/2$. This interaction recently has been formulated for metallic nanoparticles [26] and has been shown to be nonreciprocal if the particles have different dipole polarizabilities. Here, we report the complementary result for a pair of dielectric spheres when $\boldsymbol{E}_0(\boldsymbol{r})$ is linearly polarized perpendicularly to the interparticle separation $\boldsymbol{r}_{ij}$. This form of transverse optical binding is analogous to the acoustic König interaction. Appendix C adapts the Green function formalism of Ref. [27] to obtain the leading-order optical binding force,

$$\boldsymbol{F}_{ij}(\boldsymbol{r}_{ij}) = -\tfrac{3}{2}F_0 \Re\{\Phi(kr_{ij})\,\alpha_i\alpha_j^*\}\,\hat{\boldsymbol{r}}_{ij}, \tag{6a}$$

whose overall scale,

$$F_0 = k|\boldsymbol{E}_0|^2, \tag{6b}$$

is proportional to the light's intensity. As in the acoustic case, the dependence on particle separation,

$$\Phi(x) = \left(-\frac{1}{3}x^2 + ix + 1\right)\frac{e^{ix}}{x^4}, \tag{6c}$$

is structured by interference between the scattered wave and the incident wave. Assuming again that the particles are smaller than the wavelength, their leading-order coupling to the field is set by dimensionless dipole polarizabilities [28,29],

$$\alpha_i = \frac{\alpha_i^{(0)}}{1 - i\frac{\alpha_i^{(0)}}{6\pi\epsilon_0 n_0^2}}, \tag{6d}$$

where ϵ_0 is the permittivity of space, n_0 is the refractive index of the medium, and

$$\alpha_i^{(0)} = 4\pi\epsilon_0\, n_0^2\, \frac{n_i^2 - n_0^2}{n_i^2 + 2n_0^2}\,(ka_i)^3 \tag{6e}$$

is the Clausius-Mossotti polarizability for a sphere of radius a_i and refractive index n_i. Equations (6d) and (6e) are suitable for dielectric particles in the Rayleigh limit, $ka_i \ll 1$. In that limit, the leading contribution to the light-mediated interaction is proportional to $(ka_i)^3(ka_j)^3$ and is reciprocal under exchange of the particles' labels [27].

Retaining contributions to next order in the reduced size parameters, ka_i and ka_j, yields an expression,

$$\boldsymbol{F}_{ij}(\boldsymbol{r}_{ij}) = \Re\left\{\left(1 + i\chi^O_{ij}\right)\boldsymbol{F}^O_{ij}(\boldsymbol{r}_{ij})\right\}, \tag{7a}$$

that can be separated into reciprocal and nonreciprocal components, where the real part of

$$\boldsymbol{F}^O_{ij}(\boldsymbol{r}_{ij}) = -\tfrac{3}{2}F_0\,\Phi(kr_{ij})\,(\alpha_i'\alpha_j' + \alpha_i''\alpha_j'')\,\hat{\boldsymbol{r}}_{ij} \tag{7b}$$

agrees with the standard expression for the transverse optical binding force [27]. Single and double primes in Eq. (7b) refer to the real and imaginary parts of the polarizabilities, respectively. The leading nonreciprocal corrections are

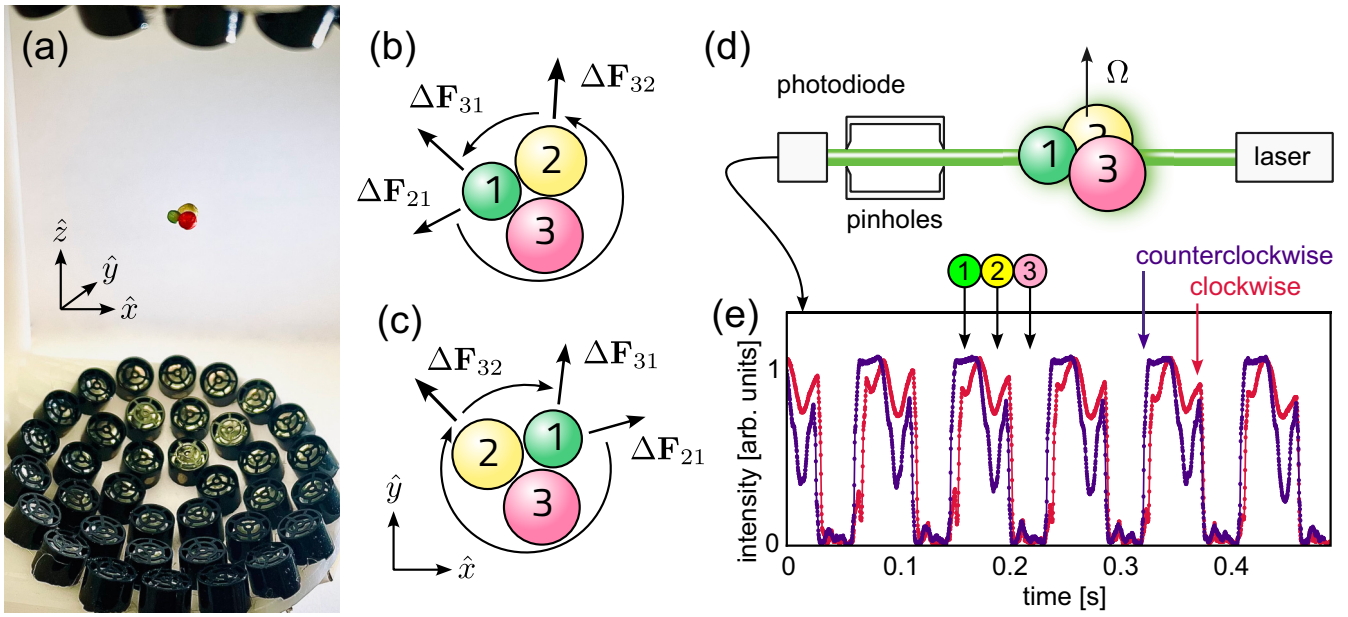

FIG. 3. Emergent activity displayed by three EPS particles levitated in an acoustic trap. (a) Photograph of the experimental system. A trio of millimeter-scale particles is trapped in a single node of a standing-wave acoustic trap at 40 kHz. (b) Schematic representation of the unbalanced forces acting on the three pairs of particles due to nonreciprocal wave-mediated interactions. The resultant torque causes the cluster to rotate about its center of mass. The cluster also would translate were it not held in place by the trap. (c) Reversing the chirality of the cluster reverses the direction of rotation. (d) Light-obscuration measurement of the cluster's rotation. A collimated laser beam is partially blocked each time a particle passes through the optical axis. The transmitted light is filtered by a pair of pinholes and its intensity is recorded with a photodiode. (e) Typical time traces of the recorded intensity for the two chiral configurations show the three particles moving through the beam in the sequence predicted in (b) and (c). The same rotation rate, $\Omega = 11(1)$ Hz, is recorded for both rotation directions.

given by

$$\chi^O_{ij} = \frac{\alpha'_i\alpha''_j - \alpha'_j\alpha''_i}{\alpha'_i\alpha'_j + \alpha''_i\alpha''_j}. \tag{7c}$$

For dielectric particles in the Rayleigh limit, the leading-order nonreciprocal corrections,

$$\chi^O_{ij} = \frac{2}{3}\frac{n_j^2 - n_0^2}{n_j^2 + 2n_0^2}(ka_j)^3 - \frac{2}{3}\frac{n_i^2 - n_0^2}{n_i^2 + 2n_0^2}(ka_i)^3, \tag{7d}$$

depend on the particles' sizes and refractive indexes and vanish appropriately if the particles are identical. The observation that $\chi^O_{ij} \neq \chi^O_{ji}$ confirms that light-mediated interactions generally are nonreciprocal. This complements the analogous result for metallic nanospheres reported in Ref. [26]. As for the acoustic interactions discussed in Sec. II A, the expression in Eq. (7) appears not to have been reported previously and predicts behavior that should be observable experimentally. Most significantly, Eq. (7) and the predictions of Ref. [26] together demonstrate that emergent activity should arise naturally in systems of particles that scatter light.

III. EXPERIMENTAL OBSERVATIONS OF EMERGENT ACTIVITY

Figure 3(a) depicts a simple experimental demonstration of emergent activity in a trio of acoustically levitated spheres. The system consists of three millimeter-scale beads of expanded polystyrene (EPS) [30] with a measured mass density [31] of $\rho_j = (30.5 \pm 0.2)\,\mathrm{kgm}^{-3}$ levitated in a standing-wave acoustic trap. The levitator is based on the standard TinyLev design [32] and consists of two banks of piezoelectric transducers (MA40S4S, Murata) operating at 40 kHz. Each bank of 36 transducers is driven harmonically at 12 V_{pp} by a software-defined function generator (ARDUINO TEENSY 4.0) and projects a traveling wave into a spherical volume of air 12.5 cm in diameter. Interference between the counterpropagating waves creates a standing wave with pressure nodes along the instrument's vertical axis $\hat{z}$.

The focused acoustic trap is more highly structured than the plane standing wave used to develop the theory of nonreciprocal wave-mediated interactions in Appendix B. Nevertheless, the experimental system shares essential features with the idealized model. An individual bead experiences one of the TinyLev's pressure nodes as a three-dimensional Hookean potential energy well [32] with a measured [31] stiffness of $5\,\mu\mathrm{Nmm}^{-1}\mathrm{V}^{-1}$ for a 1.5 mm-diameter EPS bead. The well associated with one node is large enough to contain at least three such particles. The trio in Fig. 3(a) is held in contact by a combination of the trap's primary restoring force and the beads' secondary wave-mediated interaction. The balance of forces keeps the cluster of particles rigidly trapped in the instrument's $x - y$ plane even when the instrument is inclined relative to gravity. Interference among incident and scattered waves gives rise to interparticle forces that should at least qualitatively resemble predictions of Eq. (4).

We approximate the three-particle interaction by the superposition of pairwise forces depicted in Fig. 3(b). Each of these nonreciprocal contributions is directed along one of the pair separation vectors, and therefore contributes to a

torque around the cluster's center. Of these, the unbalanced interaction between the largest and smallest beads, $\Delta \boldsymbol{F}_{31}$, is predicted by Eq. (4) to be weaker than the combined influence of the other two contributions. As a result, the cluster should experience a net torque in the $\hat{z}$ direction that causes it to rotate counterclockwise, as drawn. Indeed, the cluster is observed to rotate rapidly within its acoustic trap in the anticipated direction.

Exchanging any two beads, as illustrated in Fig. 3(c), reverses the cluster's chirality and therefore should reverse its direction of rotation. This also is observed in the experimental system. A typical realization of this experiment is presented in Supplemental Material Video 1 [33].

We measure the cluster's rotation rate using the light obscuration system depicted in Fig. 3(d). This eliminates the possibility of temporal aliasing in camera measurements due to the cluster's rapid rotation. The collimated beam from a 2 mW modular diode laser is aligned so that it is at least partially occluded when one of the particles rotates into the beam. The beam has a diameter of 2 mm, which is comparable to the diameters of the particles. Particles of different sizes can be distinguished by the proportion of the beam they block. The transmitted light passes through two coaxial 250-m-diameter pinhole apertures separated by 20 mm before being recorded by a photodiode. The photocurrent is digitized with a storage oscilloscope (TDS2002, Tektronix) at 5000 samples/s.

Typical time traces of the recorded laser intensity are plotted in Fig. 3(e) and confirm that the sense of rotation places the smallest particle in the lead, followed by the midsized particle and then the largest. For the specific trio of particles captured in Fig. 3(a), the measured rotation rate is $\Omega = 11(1)$ Hz. The cluster rotates at the same rate in either chiral configuration, which confirms that the torque results from the particles' configuration and is not somehow encoded into the structure of the acoustic trap. The cluster's rotation therefore is an example of emergent activity.

IV. EMERGENT ACTIVITY IN SIMULATED MANY-BODY SYSTEMS

To gain insight into the bulk behavior of emergently active matter, we simulate large ensembles of acoustically levitated particles. We first simulate a trio of dense spheres to confirm that the pairwise approximation at least qualitatively accounts for the experimental observations in Sec. III. We then explore larger systems to understand how nonreciprocal forces affect many-body dynamics. We simulate the dynamics of dense spheres stably levitated in an acoustic plane wave using the analytic expression for wave-mediated pair interactions, $\boldsymbol{F}^K_{ij}(\boldsymbol{r}_{ij})$, from Eq. (4). Each particle moves in the plane according to the equation of motion

$$m_i \ddot{\boldsymbol{r}}_i = -\gamma_i \dot{\boldsymbol{r}}_i + \sum_{j \neq i} \boldsymbol{F}^K_{ij}(\boldsymbol{r}_{ij}) + \frac{\varepsilon}{\sigma_{ij}} \left(1 - \frac{r_{ij}}{\sigma_{ij}}\right)^{\alpha - 1}, \quad (8)$$

with a Stokes drag coefficient, $\gamma_j = 6\pi \eta_0 a_i$, that depends on the viscosity of air, $\eta_0 = 1.8 \times 10^{-5}$ Pas [34], and where the last term describes a soft-sphere steric repulsion that prevents particle overlap ($\epsilon = 1 \times 10^5$, $\sigma_{ij} = a_i + a_j$, and $\alpha = 4$). The simulations employ a velocity Verlet integrator based on the integrator in the JAX-MD molecular dynamics engine [35]. We maintain accuracy up to single precision. We set the overall force scale to $F_0 = 10\,\mu$N, which is strong enough to rigidly confine the spheres to the plane. This drive-to-drag ratio is consistent with the forces estimated [31] for the experiments in Sec. III, with typical König interactions of 3 μN and Stokes drag per unit velocity of 0.5 N s/m. Analogous simulations of nonreciprocal optical binding in systems of dielectric spheres interacting through $\boldsymbol{F}^O_{ij}(\boldsymbol{r}_{ij})$ from Eq. (7) display emergent activity with similar phenomenology.

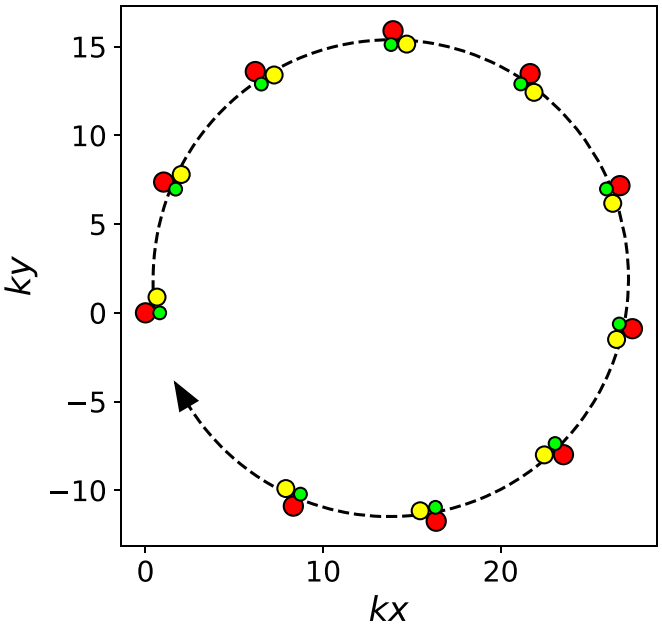

FIG. 4. Simulated trajectory of a three-particle cluster of dense spheres, translating as it rotates in the nodal plane of an acoustic standing wave. The particles' sizes and density are chosen to resemble the experimental system in Sec. III, as is the force scale F_0.

A. Three particles

To make contact with the experiments from Sec. III, we simulate a cluster of three particles that are composed of the same material but differ in size, with reduced radii of $ka_1 = 0.3$, $ka_2 = 0.5$, and $ka_3 = 0.8$. For consistency with the experimental observations, we set the density of the particles to be 30 times that of the medium [31].

Without the confining potential of the experimental acoustic trap, the simulated trio of particles translates across the nodal plane as it rotates. Figure 4 shows a typical example, and an animation rendered in INJAVIS [36] is presented in Supplemental Material Video 2 [33]. The trio's coupled rotations and translations qualitatively resemble the meandering trajectories observed in simulations of larger clusters of identical spheres [37] and experiments on self-propelled bubble pairs [38]. Both of those systems, however, rely on viscous streaming to break spatiotemporal symmetry. Motion in the present case, by contrast, unambiguously emerges from linear superposition of nonreciprocal pair interactions mediated by scattered waves.

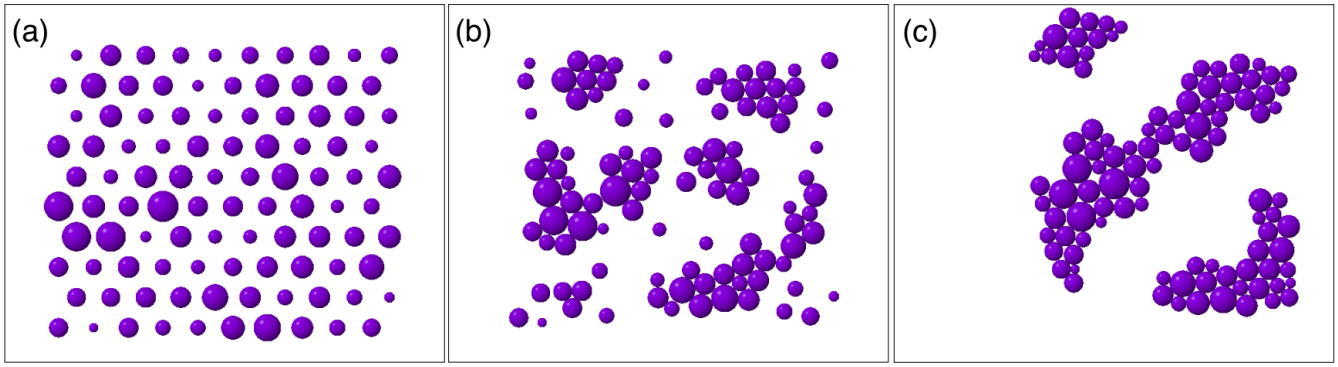

FIG. 5. Snapshots from a simulation of 100 acoustically levitated spheres with a polydispersity of $X = \sigma/\mu = 0.25$. The mean radius $k\mu = 0.4$ and force scale F_0 are chosen to reflect experimental conditions from Sec. III. (a) Particles are randomly initialized in a triangular lattice. The simulation then evolves over 10^7 time steps with a step size of 10^{-3} s. (b) Clusters rapidly coalesce under the influence of the wave-mediated König interaction. (c) Clusters display emergent activity by translating, rotating, colliding, and internally restructuring.

While the center-of-mass trajectory plotted in Fig. 4 is circular, other examples can be elliptical because the viscous drag on the cluster depends on its orientation relative to the direction of motion. Circular trajectories emerge when the rotation rate is phase locked to the center-of-mass translation.

B. Many-particle systems

The bulk behavior of emergently active systems is tuned by the heterogeneity of the particles' properties. Heterogeneity appears to be a singular perturbation to the dynamics of particle pairs. Larger ensembles may behave differently if they coalesce into configurations where nonreciprocal forces cancel and activity consequently vanishes.

We investigate collective effects in emergently active systems through simulations of acoustically levitated particles in ensembles with particle number ranging from $N = 49$ to $N = 400$. To facilitate comparison with experiments, we consider spherical particles that all have the same composition and differ only in size. We randomly draw the particles' radii from a normal distribution with a mean radius μ that we fix relative to the wavelength of sound at $k\mu = 0.4$. We vary the standard deviation of the distribution σ to study the effects of polydispersity. The system is initialized by arranging the particles in random order on a triangular lattice with lattice constant $3(\mu + \sigma)$, as shown in Fig. 5. The particles rapidly coalesce into clusters under the influence of the attractive part of the König interaction. After this initial transient, the free-floating clusters continue to translate and rotate because of unbalanced nonreciprocal interactions. A typical realization is presented in Supplemental Material Video 3 [33].

One measure of such a system's activity is provided by its rate of energy dissipation,

$$P(t) = 6\pi\eta_0 \sum_{i=1}^{N} a_i\, v_i^2(t), \tag{9}$$

where $v_i(t)$ is the translation speed of particle i at time t. This can be compared with the maximum possible dissipation rate,

$$P_0 \equiv N F_0 v_0, \tag{10}$$

for a system of N particles all moving at terminal velocity,

$$v_0 = \frac{F_0}{6\pi\eta_0\mu}, \tag{11}$$

under the influence of acoustic forces. The result is a dimensionless activity metric,

$$A(X,t) \equiv \frac{P(t)}{P_0} = \frac{1}{N}\sum_{i=1}^{N} \frac{a_i}{\mu}\left[\frac{v_i(t)}{v_0}\right]^2, \tag{12}$$

that should depend on the polydispersity, $X = \sigma/\mu$, but should be independent of system size for sufficiently large N. Once the system reaches steady state, this metric gauges the rate at which the system extracts energy from the sound wave and deposits it as heat in the fluid medium. Our activity metric thus tracks the rate of entropy production by the wave-matter composite system.

Because emergent activity is a consequence of nonreciprocal interactions, $A(X,t)$ vanishes in systems composed of identical particles ($X = 0$). Figure 6(a) shows how the activity evolves in time for systems with $N = 289$ particles and three representative values of polydispersity. In each case, the system undergoes an initial transient from a high-activity state as the particles coalesce into clusters. Once clusters have formed, each system settles into a configuration with a steady-state activity, $A_S(X)$, that depends on its polydispersity. Fluctuations in the long-time activity reflect rearrangements within clusters and collisions between clusters. The horizontal dashed lines in Fig. 6(a) are estimates for $A_S(X)$ in each of these realizations. Simulations for each value of X are repeated 15 times with different particle ensembles and system sizes to obtain estimates for the mean steady-state activity at each value of the polydispersity.

Figure 6(b) shows how the ensemble-averaged steady-state activity varies with polydispersity for acoustically levitated particle rafts of different system size N. As expected, $A_S(X)$ increases with increasing polydispersity by an amount that is independent of N for the system sizes considered. We estimate the limit of sensitivity for $A_S(X)$ by simulating systems of monodisperse particles and find it to be 10^{-14}.

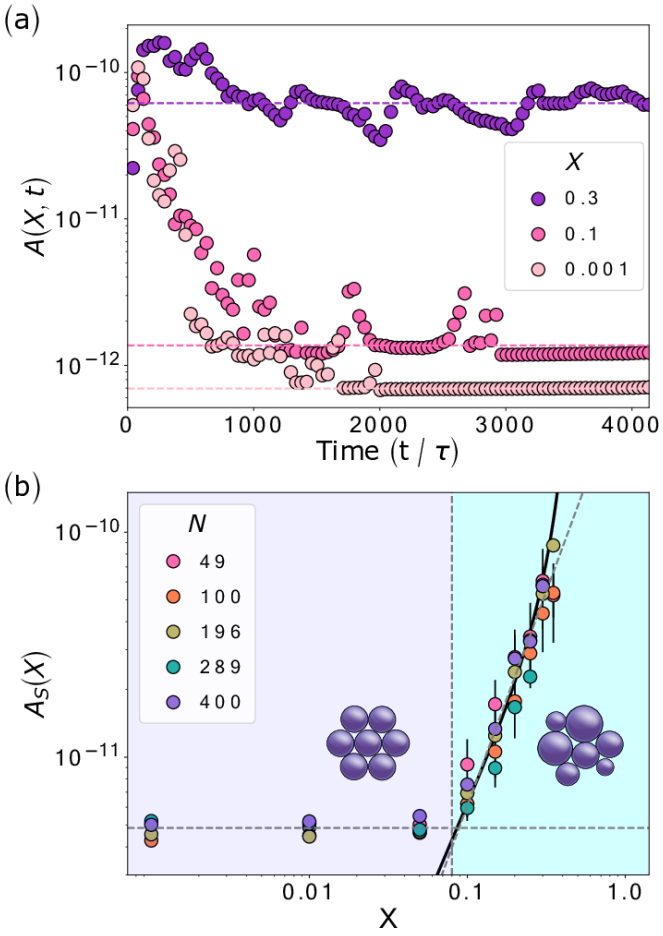

FIG. 6. (a) Simulated time evolution of the activity, $A(X,t)$, of rafts of $N = 289$ particles of mean radius $k\mu = 0.4$ in the nodal plane of an acoustic standing wave. Trajectories represent typical realizations in systems three values of polydispersity. Steady-state activities are represented by horizontal dashed lines. Time is measured in units of the viscous relaxation time $\tau = \frac{9}{2}\frac{\eta_0}{\mu^2}$. (b) Steady-state activity as a function of polydispersity. Error bars reflect the standard deviation in independent realizations. Polydisperse systems with $X > X^*$ display $A_S(X) \sim X^2$, as depicted by the gray dashed line. The two-particle prediction from Eq. (D6) is shown as a solid black curve. Insets are representative configurations for $X < X^*$ (ordered) and for $X > X^*$ (disordered).

Rafts of attractive spheres form triangular lattices at low polydispersity. The resulting sixfold symmetry favors cancellation of nonreciprocal forces and therefore tends to suppress emergent activity. Polydispersity disrupts crystalline order above $X^* \approx 0.08$ [39,40] by creating topological defects. Each such defect serves as a center for unbalanced nonreciprocal forces. The order-disorder transition therefore should enhance emergent activity for $X > X^*$. We observe this transition from a low-activity regime to a high-activity regime in Fig. 6(b), where there is a marked change in scaling at $X \approx X^*$. This transition is qualitatively similar to the dynamical phase transition between passive and active states observed in random organization models [41].

We model the activity of the emergently active state by computing the ensemble-averaged activity of pairs of dissimilar particles. Such a pair is a minimal model for the unbalanced nonreciprocal force acting on a topological defect in a close-packed raft of particles. The expectation value of the steady-state pair activity is computed in Appendix D and is expected to scale with polydispersity as

$$A_S(X) \sim X^2 \tag{13}$$

for $X < 1$. We compare this prediction for the ensemble-averaged pair activity with the observed activity, $A_S(X)$, of simulated particle rafts in Fig. 6(b), up to an overall multiplicative factor that is fit to the data. To leading order, the activity in the disordered phase scales as X^2. The analytical model agrees with simulations for $X > X^*$. Below X^*, the acoustically bound raft forms a triangular lattice without topological defects, and the residual activity is dominated by incomplete cancellation of unbalanced forces at the clusters' irregularly shaped edges.

V. DISCUSSION

We have introduced the concept of emergent activity as an organizing principle. Emergently active particles are individually passive, but become collectively active because of their nonreciprocal interactions. Nonreciprocity is known to emerge in conventionally active systems as a consequence of the individual particles' activity [42–45]. Emergent activity, conversely, is a consequence of passive particles' nonreciprocal interactions.

We have shown that nonreciprocal interactions arise naturally in systems of particles that interact by exchanging scattered waves. These nonreciprocal interactions enable the particles to exchange energy and momentum with an external field, such as a sound wave or a beam of light. Other suitable mechanisms for inducing emergent activity include streaming flows around acoustically driven bubbles [38,46,47] and wake-field interactions in dusty plasmas [48–50].

Wave-mediated interactions have the additional feature of drawing particles together into cohesive rafts without the intercession of other forces. In other systems, such as dusty plasmas, that are characterized by repulsive pair interactions, emergent activity dissipates unless an external force maintains the density of particles. In all of these cases, the degree of activity is enhanced by increasing the degree of heterogeneity in the particles' properties. For wave-mediated interactions in particular, the activity represented by the rate of entropy production appears to be proportional to the variance in the particle diameter.

In developing the phenomenology of emergent activity, we have focused on systems of particles coupled to monochromatic plane standing waves. Nonreciprocal interactions also can be fueled by more general superpositions of waves and configurations of particles. Emergent activity therefore should arise ubiquitously in any system where particles scatter waves, perhaps in combination with simple wave-mediating driving. These observations suggest that the collective motion powered by emergent activity was available to guide natural self-organization in the epoch before biological activity evolved and so could have played a role in the emergence of life.

ACKNOWLEDGMENTS

This work was supported by the National Science Foundation under Award No. DMR-2104837. E.M.K. acknowledges support from a Simons Foundation Junior Fellowship under Grant No. 1141499. We thank Marc Gershow, Jasna Brujic, Sarah Kostinski, Ankit Vyas, Mathias Casiulis, and Paul Demidov for helpful conversations.

APPENDIX A: SOUND-MEDIATED FORCES

To formulate the forces and interactions mediated by sound waves, we first introduce a multipole expansion of the Reynolds stress tensor, whose normal component quantifies the force per unit surface area exerted by a sound wave on a particle. Using this stress tensor, we first calculate the acoustic radiation force on a single spherical particle immersed in a standing wave and then the acoustic interaction force between two spheres. We use this framework to formulate the interactions between solid particles in Appendix B 2 and between bubbles in Appendix B 3.

Our system consists of discrete particles immersed in a harmonic sound wave at frequency ω whose spatial structure is described by the pressure field, $p_0(\boldsymbol{r})$. An analogous formulation can be provided for objects scattering light, water ripples, or any other harmonic wave. The total acoustic pressure field, $p(\boldsymbol{r})$, is the superposition of $p_0(\boldsymbol{r})$ and the waves scattered by particles in the system. The pressure serves as the scalar potential for the sound's velocity in a medium of density ρ_0,

$$\boldsymbol{v}(\boldsymbol{r}) = -\frac{i}{\rho_0\omega}\nabla p, \tag{A1a}$$

in the approximation that the fluid's viscosity may be neglected [13,51–53].

Both the pressure and the velocity fields contribute to the time-averaged stress tensor in the fluid medium [53,54],

$$\underline{\sigma}(\boldsymbol{r}) = \tfrac{1}{2}[\kappa_0|p(\boldsymbol{r})|^2 - \rho_0|\boldsymbol{v}(\boldsymbol{r})|^2]\underline{I} + \rho_0\,\boldsymbol{v}^*\otimes\boldsymbol{v}, \tag{A1b}$$

where $\underline{I}$ is the identity tensor and where $\kappa_0 = (\rho_0 c_0^2)^{-1}$ is the isentropic compressibility of the medium given its density and speed of sound c_0. The first term on the right-hand side of Eq. (A1b) accounts for the Lagrangian energy density of the sound. The second is the Reynolds stress [51,55]. Integrating the normal component of the stress over the surface S_i of the ith particle yields the time-averaged force experienced by that particle:

$$\boldsymbol{F}_i(\boldsymbol{r}_i) = -\frac{1}{2}\Re\left\{\oiint_{S_i}\underline{\sigma}(\boldsymbol{r})\cdot\hat{n}\,d^2r\right\}, \tag{A1c}$$

where $\hat{n}(\boldsymbol{r})$ is the unit normal to the particle's surface, and where S_i is referenced to the particle's position $\boldsymbol{r}_i$. In practice, $\boldsymbol{F}_i(\boldsymbol{r}_i)$ is most conveniently obtained by setting $p(\boldsymbol{r}) = \Pi_i(\boldsymbol{r})$ in Eq. (A1), where $\Pi_i(\boldsymbol{r})$ is the pressure inside the ith particle. We obtain an expression for this interior field by matching boundary conditions in a multipole expansion.

Referring to Fig. 2, the pressure wave incident on particle i can be expressed as

$$p_0(\boldsymbol{s}_i) = p_0\sum_{\ell=0}^{\infty}\sum_{m=-\ell}^{\ell} a_{\ell m}(k\boldsymbol{r}_i)\,j_\ell(ks_i)\,Y_\ell^m(\theta_i,\phi), \tag{A2}$$

in a spherical coordinate system, $\boldsymbol{s}_i = (s_i,\theta_i,\phi) = \boldsymbol{r} - \boldsymbol{r}_i$, centered on the particle and oriented along the pressure wave's wave vector $\hat{k}$. Distances in Eq. (A2) are scaled by the wave number in the medium, $k = \omega/c_0$. The incident wave's geometry is expressed in terms of spherical Bessel functions of the first kind, $j_\ell(kr)$, and spherical harmonics, $Y_\ell^m(\theta,\phi)$. Its structure is encoded in the beam shape coefficients, $a_{\ell m}(k\boldsymbol{r}_i)$, computed in the particle's frame of reference.

The wave scattered by particle i similarly can be expressed as a multipole expansion [56],

$$p_i(\boldsymbol{s}_i) = p_0\sum_{\ell=0}^{\infty}\sum_{m=-\ell}^{\ell} b_{\ell m}^{(i)}(k\boldsymbol{r}_i)\,h_\ell^{(1)}(ks_i)\,Y_\ell^m(\theta_i,\phi), \tag{A3}$$

in terms of spherical Hankel functions of the first kind, $h_\ell^{(1)}(kr)$. The scattered wave's beam shape coefficients,

$$b_{\ell m}^{(i)}(k\boldsymbol{r}_i) = a_{\ell m}(k\boldsymbol{r}_i)\,B_{\ell m}^{(i)}, \tag{A4}$$

are obtained from the incident wave's beam shape coefficients by applying the particle's scattering coefficients $B_{\ell m}^{(i)}$. These, in turn, are obtained by requiring the pressure and the normal component of the velocity to be continuous at the particle's surface. The same boundary conditions also yield the transmission coefficients $D_{\ell m}^{(i)}$ that establish the interior pressure,

$$\Pi_i(\boldsymbol{s}_i) = p_0\sum_{\ell=0}^{\infty}\sum_{m=-\ell}^{\ell} d_{\ell m}^{(i)}(k\boldsymbol{r}_i)\,j_\ell(k_i s_i)\,Y_\ell^m(\theta_i,\phi), \tag{A5}$$

where the interior beam shape coefficients are

$$d_{\ell m}^{(i)}(k\boldsymbol{r}_i) = a_{\ell m}(k\boldsymbol{r}_i)\,D_{\ell m}^{(i)}. \tag{A6}$$

Distances within the particle are scaled by $k_i = \omega/c_i$, where c_i is the interior speed of sound.

1. Scattering by spheres

For simplicity and clarity, we consider the special case in which the particles are spheres, each with its own radius a_i, density ρ_i, and interior speed of sound c_i. Continuity of the pressure at the ith sphere's surface requires

$$p_0(\boldsymbol{s}_i) + p_i(\boldsymbol{s}_i)|_{s_i=a_i} = \Pi_i(\boldsymbol{s}_i)|_{s_i=a_i}. \tag{A7a}$$

Continuity of the normal component of the velocity requires

$$\rho_0\frac{\partial}{\partial s_i}[p_0(\boldsymbol{s}_i) + p_i(\boldsymbol{s}_i)]\bigg|_{s_i=a_i} = \rho_i\frac{\partial}{\partial s_i}\Pi_i(\boldsymbol{s}_i)\bigg|_{s_i=a_i}. \tag{A7b}$$

In agreement with previous studies [57], we find these boundary conditions are satisfied by the scattering and transmission coefficients,

$$B_{\ell m}^{(i)} = \frac{\lambda_i\,j_\ell(ka_i)\,j_\ell'(k_ia_i) - j_\ell'(ka_i)\,j_\ell(k_ia_i)}{h_\ell^{(1)\prime}(ka_i)\,j_\ell(k_ia_i) - \lambda_i\,h_\ell^{(1)}(ka_i)\,j_\ell'(k_ia_i)}, \tag{A8}$$

$$D_{\ell m}^{(i)} = \frac{\rho_0}{\rho_i}\frac{j_\ell(ka_i)\,h_\ell^{(1)\prime}(ka_i) - j_\ell'(ka_i)\,h_\ell^{(1)}(ka_i)}{h_\ell^{(1)\prime}(ka_i)\,j_\ell(k_ia_i) - \lambda_i\,h_\ell^{(1)}(ka_i)\,j_\ell'(k_ia_i)}, \tag{A9}$$

respectively, where primes denote derivatives with respect to arguments and where $\lambda_i = \rho_0 c_0/(\rho_i c_i)$ is the specific acoustic impedance of the particle relative to that of the medium.

2. The force on a sphere

Substituting Eq. (A9) into Eq. (A5) yields the pressure within the ith sphere. The force on that sphere then follows from Eq. (A1),

$$\boldsymbol{F}_i(\boldsymbol{r}_i) = F_0\,\Re\left\{\sum_{\ell=0}^{\infty}\sum_{m=-\ell}^{\ell} J_{\ell m}^{(i)}\, d_{\ell m}^{(i)}\, d_{\ell+1,m}^{(i)*}\right\}\hat{k}. \tag{A10}$$

The magnitude of the force is set by a prefactor,

$$F_0 = \frac{p_0^2}{\rho_0\,\omega^2}, \tag{A11}$$

that depends on properties of the sound wave in the medium. Coupling between multipole moments mediated by scattering at the sphere's surface is described by the coefficients

$$J_{\ell m}^{(i)} = \frac{1}{2}\left(\frac{\rho_i}{\rho_0}\right)^2\sqrt{\frac{(\ell-m+1)(\ell+m+1)}{(2\ell+3)(2\ell+1)}}\left\{[m^2-(ka_i)^2]\,j_\ell(x_i)\,j_{\ell+1}(x_i)\right.$$
$$\left.+\frac{\rho_0}{\rho_i}x_i[\ell\,j_\ell(x_i)\,j'_{\ell+1}(x_i)-(\ell+2)\,j'_\ell(x_i)\,j_{\ell+1}(x_i)]-\left(\frac{\rho_0}{\rho_i}x_i\right)^2 j'_\ell(x_i)\,j'_{\ell+1}(x_i)\right\}, \tag{A12}$$

where $x_i = k_i a_i$. Equation (A12) differs from previously reported expressions [51,54,56] for the coupling coefficients $J_{\ell m}^{(i)}$, which only include terms with $m = 0$. The additional terms in the complete expression are required for waves that lack azimuthal symmetry, including the scattered waves exchanged by pairs of particles. Equation (A12) is analogous to Eq. (2.32) in Ref. [57], but projects the force along $\hat{k}$ rather than $\hat{z}$, which is more useful for computing interactions.

3. A sphere in a standing wave

As an illustrative example, we use this formalism to evaluate the force exerted on the ith sphere by a plane standing wave,

$$p_0(\boldsymbol{r}) = p_0\sin(kz), \tag{A13}$$

whose axis is aligned in the vertical direction $\hat{z}$. The incident field's beam shape coefficients [53,56],

$$a_{\ell m}^{(0)}(k\boldsymbol{r}_i) = 4\pi(-1)^{\ell-m}\sin\left(kz_i-\ell\frac{\pi}{2}\right)Y_\ell^{-m}(\alpha,0), \tag{A14}$$

depend on the particle's height z_i above the nodal plane at $z = 0$. Referring to the coordinate system from Fig. 2, the $\hat{z}$-oriented incident wave has $\alpha = 0$. In the absence of other particles, we can use Eq. (A10) to compute the force on particle i due to the incident field:

$$\boldsymbol{F}_i(\boldsymbol{r}_i) = \frac{\pi}{3}F_0\,(ka_i)^3\left(\frac{\kappa_i}{\kappa_0}-\frac{3\rho_i}{\rho_0+2\rho_i}\right)\sin(2kz_i)\,\hat{z}. \tag{A15}$$

Equation (A15) includes only terms at monopole order ($\ell = 0$) in the multipole expansion, and agrees with the standard Gor'kov expression [57] for the leading-order acoustic trapping force. Contributions from higher multipole terms, $\ell \geqslant 1$, appear at order $(ka_j)^5$ in the dimensionless particle size and therefore can be neglected for spheres that are smaller than the wavelength of sound, $ka_j < 1$.

The Gor'kov force vanishes at both nodes and antinodes of the incident pressure wave. The prefactor of $\boldsymbol{F}_i$ is negative for dense spheres ($\rho_i < \rho_0$ and $\kappa_i > \kappa_0$). Such particles are stably trapped at pressure nodes. Bubbles, by contrast, are stably trapped at antinodes. This distinction qualitatively differentiates the acoustic force landscape experienced by dense spheres and bubbles. It also establishes qualitatively different contexts for their wave-mediated interactions.

APPENDIX B: SOUND-MEDIATED PAIR INTERACTIONS

1. Acoustic forces on a pair of particles

As illustrated schematically in Fig. 2, the wave scattered by particle j interferes with the external wave incident on particle i,

$$p(\boldsymbol{r}) = p_0(\boldsymbol{r}) + p_j(\boldsymbol{r}-\boldsymbol{r}_j), \tag{B1}$$

and therefore contributes to the force experienced by particle i. In principle, the second particle scatters a portion of $p(\boldsymbol{r})$ back to the first, giving rise to a hierarchy of exchanged waves. For simplicity, we invoke the first Born approximation and consider only the first exchange of scattered waves.

Computing the force on particle i requires an expression for the interior pressure, $\Pi_i(\boldsymbol{r})$, and thus an expression for the first particle's scattered wave, $p_j(\boldsymbol{r}-\boldsymbol{r}_j)$, in spherical coordinates $\boldsymbol{s}_i$ centered on $\boldsymbol{r}_i$. To facilitate the projection, we align the axis of the coordinate system along $\boldsymbol{r}_{ij} = \boldsymbol{r}_i - \boldsymbol{r}_j$, as shown in Fig. 2, and set the angle α in Eq. (A14) accordingly. In this coordinate system, the pressure wave scattered by particle j,

$$p_j(\boldsymbol{s}_i) = p_0\sum_{\ell=0}^{\infty}\sum_{m=-\ell}^{\ell} a_{\ell m}^{(ij)}\,j_\ell(ks_i)\,Y_\ell^m(\theta_i,\phi), \tag{B2}$$

is incident on particle i with beam shape coefficients,

$$a_{\ell m}^{(ij)} = \sum_{n=0}^{\infty} K_{n\ell m}(kr_{ij})\,b_{nm}^{(j)}(k\boldsymbol{r}_j), \tag{B3a}$$

that are projected from the scattered wave's coefficients with a projection kernel [58],

$$K_{n\ell m}(kr_{ij}) = \sum_{s=0}^{\ell+n}\sqrt{\frac{2s+1}{4\pi}}\,C(nm|s0|\ell m)\,h_s^{(1)}(kr_{ij}), \tag{B3b}$$

that accounts for the particles' separation, $r_{ij} = |\boldsymbol{r}_{ij}|$. The projection coefficients are expressed in terms of Wigner 3-j

symbols through

$$C(nm|s0|\ell m) = i^{-n+s+\ell}(-1)^m\sqrt{4\pi(2\ell+1)(2s+1)(2n+1)} \times \begin{pmatrix} n & s & \ell \\ 0 & 0 & 0 \end{pmatrix}\begin{pmatrix} n & s & \ell \\ -m & 0 & m \end{pmatrix}. \tag{B3c}$$

The upper limit of the sum in Eq. (B3b) reflects selection rules for the Wigner 3-j symbols [59].

Both the incident and scattered waves contribute to the beam shape coefficients for the wave inside particle i,

$$d_{\ell m}^{(ij)} = \left(a_{\ell m}^{(0)} + a_{\ell m}^{(ij)}\right)D_{\ell m}^{(i)}. \tag{B4}$$

The particle's size and properties influence the interior wave through the transmission coefficients from Eq. (A9). The net wave-mediated force on particle i then follows from Eq. (A10). The complementary force on the neighboring particle is obtained by exchanging labels i and j.

The total force experienced by particle i includes contributions from the incident wave, the scattered wave, and their interference. To clarify the nature of the interparticle interaction, we assume that both particles are stably trapped in the same nodal plane of the planar standing wave described by Eq. (A13). The primary Gor'kov force therefore vanishes identically and $a_{\ell m}^{(0)}(k\boldsymbol{r})$ from Eq. (A14) is evaluated at $z = 0$ and with $\alpha = \pi/2$ for both particles. The acoustic force on particle i therefore can be attributed entirely to its wave-mediated interaction with particle j,

$$\boldsymbol{F}_{ij}(\boldsymbol{r}_{ij}) = F_0\,\Re\left\{\sum_{\ell=0}^{\infty}\sum_{m=-\ell}^{\ell} J_{\ell m}^{(i)}\, d_{\ell m}^{(ij)}\, d_{\ell+1,m}^{(ij)*}\right\}\hat{\boldsymbol{r}}_{ij}. \tag{B5}$$

For this much-studied model system [14,16,51,54,60,61], the wave-mediated force depends on the particles' separation through the beam-shape coefficients $d_{\ell m}^{(ij)}$.

The pair interaction in this geometry historically has been dubbed the König force for dense spheres [14] and the secondary Bjerknes interaction for bubbles [60]. For simplicity, we formulate this force in the Rayleigh approximation, $ka_i, ka_j < 1$, so that we may reasonably truncate the multipole expansion at quadrupole order, $\ell = 2$.

2. König interaction: Dense spheres in a standing plane wave

Spheres that are denser than the fluid medium will be localized in one of the nodal planes of the standing wave. The leading-order expression for the wave-mediated force on particle i due to particle j,

$$\boldsymbol{F}_{ij}^{K}(\boldsymbol{r}) = -2\pi\, F_0\, \Phi_K(kr)\, \eta_i\eta_j\, \hat{\boldsymbol{r}}, \tag{B6a}$$

is the König interaction [14]. Its dependence on the particles separation,

$$\Phi_K(kr) = \frac{\left[1 - \frac{1}{3}(kr)^2\right]\cos(kr) + kr\sin(kr)}{(kr)^4}, \tag{B6b}$$

shows that the wave-mediated interaction is attractive when the particles are near contact and changes sign at larger separations. The particles' coupling constants [62],

$$\eta_i = \frac{\rho_0 - \rho_i}{\rho_0 + 2\rho_i}(ka_i)^3, \tag{B6c}$$

depend on their density mismatch with the medium, but not on their compressibilities. This is reasonable because dense particles principally scatter the dipolar velocity field.

Equation (B6) reduces to the previously published form for the pair interaction [16] in the special case of identical particles. The asymmetric case appears not to have been reported previously.

Most previous studies of sound-mediated pair interactions go no further than the dipole approximation and conclude that wave-mediated interactions are reciprocal in general [56,57]. References [16] and [37] note the existence of nonreciprocal acoustic interactions between pairs of bubbles but suggest they are too small to be significant. In fact, the nature of the pair interaction changes qualitatively when higher-order multipole contributions are taken into account. These changes are present even in the first-scattering approximation, and take a surprisingly elegant form.

The leading quadrupole-order correction to the König force,

$$\boldsymbol{F}_{ij}(\boldsymbol{r}) = \boldsymbol{F}_{ij}^{K}(\boldsymbol{r})\,(1 + \chi_{ij}^{K}), \tag{B7}$$

breaks the reciprocity of the pair interaction with a term,

$$\chi_{ij}^{K} = \alpha_{ij}^{K} + \beta_{ij}^{K}\,(ka_i)^2 + \gamma_{ij}^{K}\,(ka_j)^2, \tag{B8a}$$

that identifies roles for the spheres' sizes and compositions through the coefficients

$$\alpha_{ij}^{K} = -\frac{2}{3}\frac{\rho_0}{\rho_i} \tag{B8b}$$

$$\beta_{ij}^{K} = -\frac{3}{10}\left(1 - \frac{\kappa_j}{\kappa_0} + \frac{3}{2}\frac{\rho_0}{\rho_j} - \frac{2}{3}\frac{\rho_0}{\rho_i}\right) \tag{B8c}$$

$$\gamma_{ij}^{K} = -\frac{19}{18} + \frac{127}{210}\frac{\kappa_i}{\kappa_0} - \frac{67}{108}\frac{\rho_0}{\rho_i}. \tag{B8d}$$

Equation (B8) establishes the conditions under which acoustically levitated spheres experience nonreciprocal interactions. Because $\alpha_{ij}^{K} \neq \alpha_{ji}^{K}$, spheres with different densities interact nonreciprocally even if they have the same size. The different functional forms of β_{ij}^{K} and γ_{ij}^{K} have the consequence that spheres of different sizes interact nonreciprocally even if they are made of the same material. Equation (B8) further reveals that nonreciprocal effects should be most prominent for particles that are comparable in size to the wavelength of sound, $ka_i \lesssim 1$, and are nearly density-matched to the medium, $\rho_i \gtrsim \rho_0$.

3. Bjerknes interaction: Bubbles in a standing plane wave

Bubbles are less dense than the medium ($\rho_i < \rho_0$) and more compressible ($\kappa_i > \kappa_0$) and so are localized at antinodes of the pressure wave. The wave-mediated force between acoustically levitated bubbles is commonly known as the secondary Bjerknes interaction [60] and broadly resembles the König interaction between dense spheres from Eq. (B6). To leading nontrivial order in the small parameters ka_i, ρ_i/ρ_0, and κ_0/κ_i, Eq. (B5) predicts that the wave-mediated interaction between two bubbles separated by distance r in an antinodal plane of a standing wave is

$$\boldsymbol{F}_{ij}^{B}(\boldsymbol{r}) = -\frac{2\pi}{9}\, F_0\, \Phi_B(kr)\, \eta_i\eta_j\, \hat{\boldsymbol{r}}, \tag{B9a}$$

with coupling constants of the form [62]

$$\eta_i = \left(1 - \frac{\kappa_i}{\kappa_0}\right)(ka_i)^3. \tag{B9b}$$

The Bjerknes interaction is longer-ranged than the König interaction,

$$\Phi_B(kr) = \frac{\cos(kr) + kr\,\sin(kr)}{(kr)^2}, \tag{B9c}$$

and is attractive at short ranges. Bubbles' coupling constants depend on their compressibilities rather than their densities because bubbles principally scatter the pressure field, with a leading contribution from monopole scattering. Equation (B9) includes terms up to dipole order ($\ell = 1$) in the multipole expansion and agrees with previously reported expressions [54,57] for this interaction at the same level of approximation. Reference [51] proposes a different numerical prefactor because its derivation imposes axisymmetry on the pressure field, which is not appropriate for multipole contributions with $m \neq 0$. As for the König interaction between dense spheres, the leading-order Bjerknes interaction is reciprocal, $\boldsymbol{F}^B_{21}(r) = -\boldsymbol{F}^B_{12}(r)$, even for bubbles of different sizes and compositions.

The quadrupole-order expression,

$$\boldsymbol{F}_{ij}(\boldsymbol{r}) = \boldsymbol{F}^B_{ij}(\boldsymbol{r})\left(1 + \chi^B_{ij}\right), \tag{B10}$$

introduces a correction,

$$\chi^B_{ij} = \alpha^B_{ij} + \beta^B_{ij}\,(ka_j)^2 + \gamma^B_{ij}\,(ka_i)^2, \tag{B11a}$$

that depends on the bubbles' compositions and sizes. Additional terms and higher multipole contributions all appear at $\mathcal{O}\{(ka_j)^3\}$ or $\mathcal{O}\{(ka_i)^3\}$ and so can be neglected in the Rayleigh approximation. Expressing the coefficients to leading nontrivial order yields

$$\alpha^B_{ij} = -\frac{3}{2}\frac{\kappa_0}{\kappa_i}\frac{\rho_i^2}{\rho_0^2} \tag{B11b}$$

$$\beta^B_{ij} = -\frac{2}{3} + \frac{1}{3}\frac{\kappa_j}{\kappa_0}\left(1 + \frac{1}{5}\frac{\rho_j}{\rho_0}\right) \tag{B11c}$$

$$\gamma^B_{ij} = -\frac{2}{3} + \frac{1}{3}\frac{\kappa_i}{\kappa_0}\left(1 + \frac{1}{5}\frac{\rho_i}{\rho_0}\right), \tag{B11d}$$

from which we conclude the wave-mediated interactions between pairs of bubbles are reciprocal unless the bubbles are composed of different materials. Size-dependent nonreciprocity emerges at higher orders in the small parameters, ρ_i/ρ_0, ρ_j/ρ_0, κ_0/κ_i, and κ_0/κ_j. Comparing Eq. (B11b) with Eq. (B8b) suggests that $\alpha^B_{ij} \ll \alpha^K_{ij}$, which means that composition-dependent nonreciprocity should be significantly weaker for bubbles than for dense particles. This is consistent with earlier reports [16,37]. Nonreciprocal effects should be most evident in systems such as emulsions where the "bubbles" are nearly density matched to the medium and have comparable compressibility. The nature of the pairwise nonreciprocity reported in Eqs. (B8) and (B11) complements a recent report of nonreciprocal wave-mediated interactions that arise from the viscosity of the medium thanks to streaming effects that we do not consider [38].

APPENDIX C: LIGHT-MEDIATED PAIR INTERACTIONS

The electric field acting on a dielectric particle at position $\boldsymbol{r}_i$ is the superposition of the incident field, $\boldsymbol{E}_0(\boldsymbol{r})$, and the field scattered by its neighbor at $\boldsymbol{r}_j$:

$$\boldsymbol{E}_i(\boldsymbol{r}_i) = \boldsymbol{E}_0(\boldsymbol{r}_i) + \alpha_j\,\boldsymbol{E}_j(\boldsymbol{r}_j)\,\underline{G}(\boldsymbol{r}_{ij}), \tag{C1}$$

where α_j is the scattering coefficient for particle j, $\boldsymbol{E}_j(\boldsymbol{r}_j)$ is the total field incident on particle j, and $\boldsymbol{r}_{ij} = \boldsymbol{r}_i - \boldsymbol{r}_j$ is the interparticle separation. The tensorial Green function [27],

$$\underline{G}(\boldsymbol{r}) = [\lambda(r) - \mu(r)]\,\hat{\boldsymbol{r}} \otimes \hat{\boldsymbol{r}} + \mu(r)\,\underline{I}, \tag{C2}$$

expresses propagation of the components of the scattered wave from j to i in terms of the partial waves

$$\lambda(r) = \frac{e^{ikr}}{r^3}(1 - ikr) \tag{C3}$$

and

$$\mu(r) = \frac{e^{ikr}}{r^3}[(kr)^2 - 1 + ikr]. \tag{C4}$$

For simplicity, we assume that the incident field is uniform, $\boldsymbol{E}_0(\boldsymbol{r}) = \boldsymbol{E}_0$. When the incident field is linearly polarized either transverse or parallel to $\boldsymbol{r}_{ij}$, the magnitude of the field incident on particle i can be expressed self-consistently as

$$E_i(\boldsymbol{r}_i) = E_0\,\frac{1 + \alpha_j\,G_{ij}}{1 - \alpha_i\alpha_j\,G^2_{ij}(\boldsymbol{r}_{ij})}, \tag{C5}$$

where G_{ij} is the transverse or longitudinal component of $\underline{G}(\boldsymbol{r}_{ij})$, respectively.

The total force on particle i due to particle j follows from the field [63]

$$\boldsymbol{F}_i(\boldsymbol{r}_i) = \frac{1}{2}\sum_{n=1}^{3}\Re\left\{\alpha_i^*\,E^*_{i,n}\frac{\partial E_{i,n}}{\partial r}\right\}\hat{e}_n, \tag{C6}$$

where the subscript n refers to the Cartesian coordinates. This expression includes the pair interaction,

$$\boldsymbol{F}_{ij}(\boldsymbol{r}_{ij}) = \frac{1}{2}E_0^2\Re\left\{\alpha_i^*\alpha_j(1 + 2\alpha_i G_{ij} + \alpha_j^* G_{ij}^*)\frac{\partial G_{ij}}{\partial r}\right\}\hat{r}_{ij} + \mathcal{O}\{\alpha_i\alpha_j G_{ij}^2\}, \tag{C7}$$

which we express in the limit of weak scattering, $|\alpha_j G_{ij}| \ll 1$. Specializing to the case of transverse polarization, $G_{ij} = \lambda(r_{ij})$, we obtain an expression for the pair interaction,

$$\boldsymbol{F}_{ij}(\boldsymbol{r}_{ij}) = -\frac{3}{2}E_0^2\,\Re\left\{\alpha_i^*\alpha_j\left[-\frac{(kr_{ij})^2}{3} + ikr_{ij} + 1\right]e^{ikr_{ij}}\right\}\hat{r} + \mathcal{O}\{k^6\alpha_i^3\}. \tag{C8}$$

Factoring the separation dependence into $\Phi(kr)$ yields the expression for the optical binding force presented in Eq. (6). The reciprocal part of the interaction is obtained by noting that the product of particle polarizabilities can be written as

$$\alpha_i^* \alpha_j = \alpha_i' \alpha_j' + \alpha_i'' \alpha_j'' + i(\alpha_i' \alpha_j'' - \alpha_i'' \alpha_j') \tag{C9}$$

and taking the real part. The nonreciprocal component comes from the imaginary part. We can then write the optical binding force in the form of Eq. (7b). The final expression is obtained by applying Eqs. (6d) and (6e) and neglecting terms of higher order than $\mathcal{O}\{k^6 a_i^6\}$.

APPENDIX D: ACTIVITY AS A FUNCTION OF POLYDISPERSITY

The steady-state velocity of a pair of acoustically levitated particles arises from the competition between unbalanced center-of-mass forces and viscous drag. Hydrodynamic coupling reduces the drag on a pair of spheres [64] relative to the sum of Stokes contributions, which means that

$$\boldsymbol{v}_{ij} = \frac{\chi_{ij} - \chi_{ji}}{6\pi\eta_0 (a_i + a_j)} F_{ij}^K (a_i + a_j)\, \hat{\boldsymbol{r}}_{ij} \tag{D1}$$

is an underestimate for the pair velocity due to emergent activity. Equations (12) and (B8b) then suggest that two dense spheres composed of the same material have an emergent activity that depends on their composition and sizes as

$$A_S(a_i, a_j) \approx \frac{3}{2}\pi^2 f_1^4\, k\mu\, (k a_i)^7\, \xi^6\, \frac{(1-\xi)^2}{(1+\xi)^7}, \tag{D2}$$

where

$$f_1 = \frac{\rho_0 - \rho_i}{\rho_0 + 2\rho_i} \tag{D3}$$

is the dipole polarizability of a sphere of density ρ_i and $\xi = a_j/a_i$ is the spheres' size ratio.

We compute the ensemble-averaged pair activity by assuming that the spheres' radii are drawn from a Gamma distribution,

$$p(a) = \frac{1}{a}\left(\frac{\mu a}{\sigma^2}\right)^{\frac{\mu^2}{\sigma^2}} \frac{e^{-\frac{\mu a}{\sigma^2}}}{\Gamma\left(\frac{\mu^2}{\sigma^2}\right)}, \tag{D4}$$

with mean μ and variance σ^2. Under this assumption, ξ is an independent random variable that is drawn from the Beta prime distribution with probability density

$$p(\xi) = \frac{\xi^{-1+\frac{\mu^2}{\sigma^2}} (1+\xi)^{-2\frac{\mu^2}{\sigma^2}}}{B\left(\frac{\mu^2}{\sigma^2}, \frac{\mu^2}{\sigma^2}\right)}. \tag{D5}$$

Averaging Eq. (D2) over $a_i \in [0, \infty]$ and over $\xi \in [0, 1]$ yields the mean pair activity,

$$A_S(X) = A_0 X^{14} \frac{\Gamma\left(6 + \frac{1}{X^2}\right)\Gamma\left(7 + \frac{1}{X^2}\right)\Gamma\left(\frac{2}{X^2}\right)}{\Gamma\left(9 + \frac{1}{X^2}\right)\Gamma^3\left(\frac{1}{X^2}\right)} \times -6 + \frac{1}{X^2}, 7 + \frac{2}{X^2}; 9 + \frac{1}{X^2}; -1, \tag{D6a}$$

as a function of the polydispersity, $X = \mu/\sigma$. The activity is expressed in terms of the gamma function, $\Gamma(n)$, and the Gauss hypergeometric function, $-a, b; c; z$. The overall activity scale,

$$A_0 \approx \frac{3}{2}\pi^2 f_1^4 (k\mu)^8, \tag{D6b}$$

depends strongly on the mean particle size μ relative to the wavelength.

We obtain the leading-order scaling of emergent activity as a function of polydispersity through a mean field approximation. We assume that the radius of each particle differs only slightly from the mean, $a_i = \mu(1 + \epsilon_i)$, and that ϵ_i is drawn from a normal distribution with width σ/μ. The emergent activity of two dense spheres is then

$$A_S(a_i, a_j) = A_0 \frac{(1+\epsilon_i)^6 (1+\epsilon_j)^6 (\epsilon_i - \epsilon_j)^2}{(2 + \epsilon_i + \epsilon_j)^7}. \tag{D7}$$

Applying the binomial expansion to the denominator under the assumption that $\epsilon_i + \epsilon_j \ll 2$, and averaging the resulting polynomial expression over ϵ_i and ϵ_j then yields the leading-order behavior

$$A_S(X) = A_0(X^2 + \mathcal{O}\{X^4\}) \tag{D8}$$

that appears in Eq. (13).

[1] S. Ramaswamy, The mechanics and statistics of active matter, Annu. Rev. Condens. Matter Phys. **1**, 323 (2010).

[2] M. C. Marchetti, J.-F. Joanny, S. Ramaswamy, T. B. Liverpool, J. Prost, M. Rao, and R. A. Simha, Hydrodynamics of soft active matter, Rev. Mod. Phys. **85**, 1143 (2013).

[3] C. Bechinger, R. Di Leonardo, H. Löwen, C. Reichhardt, G. Volpe, and G. Volpe, Active particles in complex and crowded environments, Rev. Mod. Phys. **88**, 045006 (2016).

[4] S. Shankar, A. Souslov, M. J. Bowick, M. C. Marchetti, and V. Vitelli, Topological active matter, Nat. Rev. Phys. **4**, 380 (2022).

[5] D. Needleman and Z. Dogic, Active matter at the interface between materials science and cell biology, Nat. Rev. Mater. **2**, 17048 (2017).

[6] J. Palacci, S. Sacanna, A. P. Steinberg, D. J. Pine, and P. M. Chaikin, Living crystals of light-activated colloidal surfers, Science **339**, 936 (2013).

[7] N. C. Darnton, L. Turner, S. Rojevsky, and H. C. Berg, Dynamics of bacterial swarming, Biophys. J. **98**, 2082 (2010).

[8] A. Cavagna and I. Giardina, Bird flocks as condensed matter, Annu. Rev. Condens. Matter Phys. **5**, 183 (2014).

[9] Z. You, A. Baskaran, and M. C. Marchetti, Nonreciprocity as a generic route to traveling states, Proc. Natl. Acad. Sci. USA **117**, 19767 (2020).

[10] R. Soto and R. Golestanian, Self-assembly of catalytically active colloidal molecules: Tailoring activity through surface chemistry, Phys. Rev. Lett. **112**, 068301 (2014).

[11] M. Brandenbourger, X. Locsin, E. Lerner, and C. Coulais, Non-reciprocal robotic metamaterials, Nat. Commun. **10**, 4608 (2019).

[12] H. Bruus, Acoustofluidics 7: The acoustic radiation force on small particles, Lab Chip **12**, 1014 (2012).

[13] M. A. Abdelaziz and D. G. Grier, Acoustokinetics: Crafting force landscapes from sound waves, Phys. Rev. Res. **2**, 013172 (2020).

[14] W. König, Hydrodynamisch-akustische Untersuchungen, Ann. Phys. **279**, 43 (1891).

[15] M. A. H. Weiser, R. E. Apfel, and E. A. Neppiras, Interparticle forces on red cells in a standing wave field, Acta Acust. Acust. **56**, 114 (1984).

[16] G. T. Silva and H. Bruus, Acoustic interaction forces between small particles in an ideal fluid, Phys. Rev. E **90**, 063007 (2014).

[17] Y. A. Kobelev, L. Ostrovskii, and A. Sutin, Self-illumination effect for acoustic waves in a liquid with gas bubbles, JETP Lett. **30**, 395 (1979).

[18] R. E. Apfel, Y. Zheng, and Y. Tian, Studies of acousto-electrically levitated drop and particle clusters and arrays, J. Acoust. Soc. Am. **105**, L1 (1999).

[19] D. Rabaud, P. Thibault, M. Mathieu, and P. Marmottant, Acoustically bound microfluidic bubble crystals, Phys. Rev. Lett. **106**, 134501 (2011).

[20] M. A. Abdelaziz, J. A. Díaz A, J.-L. Aider, D. J. Pine, D. G. Grier, and M. Hoyos, Ultrasonic chaining of emulsion droplets, Phys. Rev. Res. **3**, 043157 (2021).

[21] M. X. Lim, A. Souslov, V. Vitelli, and H. M. Jaeger, Cluster formation by acoustic forces and active fluctuations in levitated granular matter, Nat. Phys. **15**, 460 (2019).

[22] M. X. Lim, B. VanSaders, A. Souslov, and H. M. Jaeger, Mechanical properties of acoustically levitated granular rafts, Phys. Rev. X **12**, 021017 (2022).

[23] K. Y. Bliokh and F. Nori, Spin and orbital angular momenta of acoustic beams, Phys. Rev. B **99**, 174310 (2019).

[24] M. M. Burns, J.-M. Fournier, and J. A. Golovchenko, Optical binding, Phys. Rev. Lett. **63**, 1233 (1989).

[25] K. Dholakia and P. Zemánek, *Colloquium:* Gripped by light: Optical binding, Rev. Mod. Phys. **82**, 1767 (2010).

[26] S. Sukhov, A. Shalin, D. Haefner, and A. Dogariu, *Actio et reactio* in optical binding, Opt. Express **23**, 247 (2015).

[27] F. Dapasse and J.-M. Vigoureux, Optical binding force between two Rayleigh particles, J. Phys. D: Appl. Phys. **27**, 914 (1994).

[28] B. T. Draine and J. Goodman, Beyond Clausius-Mossotti: Wave propagation on a polarizable point lattice and the discrete dipole approximation, Astrophys. J. **405**, 685 (1993).

[29] S. Albaladejo, R. Gómez-Medina, L. S. Froufe-Pérez, H. Marinchio, R. Carminati, J. Torrado, G. Armelles, A. García-Martín, and J. J. Sáenz, Radiative corrections to the polarizability tensor of an electrically small anisotropic dielectric particle, Opt. Express **18**, 3556 (2010).

[30] J. Horvath, Expanded polystyrene (EPS) geofoam: An introduction to material behavior, Geotext. Geomembr. **13**, 263 (1994).

[31] M. Morrell and D. G. Grier, Acoustodynamic mass determination: Accounting for inertial effects in acoustic levitation of granular materials, Phys. Rev. E **108**, 064903 (2023).

[32] A. Marzo, A. Barnes, and B. W. Drinkwater, TinyLev: A multi-emitter single-axis acoustic levitator, Rev. Sci. Instrum. **88**, 085105 (2017).

[33] See Supplemental Material at http://link.aps.org/supplemental/10.1103/PhysRevResearch.7.013055 for videos of experimental and simulated observations of emergent activity in clusters of particles scattering sound waves and light waves.

[34] *CRC Handbook of Chemistry and Physics*, 104th ed., edited by D. Lide (Taylor & Francis, Abingdon, 2017).

[35] S. S. Schoenholz and E. D. Cubuk, JAX, M.D. A framework for differentiable physics, J. Stat. Mech. (2021) 124016.

[36] M. Engel, INJAVIS — INteractive JAva VISualization, Zenodo, 4639570 (2021).

[37] N. St. Clair, D. Davenport, A. D. Kim, and D. Kleckner, Dynamics of acoustically bound particles, Phys. Rev. Res. **5**, 013051 (2023).

[38] A. A. Doinikov, T. Micol, C. Mauger, P. Blanc-Benon, and C. Inserra, Self-propulsion of two contacting bubbles due to the radiation interaction force, Micromachines **14**, 1615 (2023).

[39] P. Pusey, E. Zaccarelli, C. Valeriani, E. Sanz, W. C. Poon, and M. E. Cates, Hard spheres: Crystallization and glass formation, Philos. Trans. R. Soc. A **367**, 4993 (2009).

[40] S. Pronk and D. Frenkel, Melting of polydisperse hard disks, Phys. Rev. E **69**, 066123 (2004).

[41] S. Wilken, R. E. Guerra, D. Levine, and P. M. Chaikin, Random close packing as a dynamical phase transition, Phys. Rev. Lett. **127**, 038002 (2021).

[42] A. Furukawa, D. Marenduzzo, and M. E. Cates, Activity-induced clustering in model dumbbell swimmers: The role of hydrodynamic interactions, Phys. Rev. E **90**, 022303 (2014).

[43] S. Saha, S. Ramaswamy, and R. Golestanian, Pairing, waltzing and scattering of chemotactic active colloids, New J. Phys. **21**, 063006 (2019).

[44] M. Fruchart, R. Hanai, P. B. Littlewood, and V. Vitelli, Non-reciprocal phase transitions, Nature (London) **592**, 363 (2021).

[45] D. J. Hickey, R. Golestanian, and A. Vilfan, Nonreciprocal interactions give rise to fast cilium synchronization in finite systems, Proc. Natl. Acad. Sci. USA **120**, e2307279120 (2023).

[46] D. Ahmed, M. Lu, A. Nourhani, P. E. Lammert, Z. Stratton, H. S. Muddana, V. H. Crespi, and T. J. Huang, Selectively manipulable acoustic-powered microswimmers, Sci. Rep. **5**, 9744 (2015).

[47] T. Luo and M. Wu, Biologically inspired micro-robotic swimmers remotely controlled by ultrasound waves, Lab Chip **21**, 4095 (2021).

[48] E. Lisin, O. Petrov, E. Sametov, O. Vaulina, K. Statsenko, M. Vasiliev, J. Carmona, and T. Hyde, Experimental study of the nonreciprocal effective interactions between microparticles in an anisotropic plasma, Sci. Rep. **10**, 13653 (2020).

[49] A. D. Usachev, A. V. Zobnin, O. F. Petrov, V. E. Fortov, B. M. Annaratone, M. H. Thoma, H. Höfner, M. Kretschmer, M. Fink, and G. E. Morfill, Formation of a boundary-free dust cluster in a low-pressure gas-discharge plasma, Phys. Rev. Lett. **102**, 045001 (2009).

[50] A. V. Ivlev, J. Bartnick, M. Heinen, C.-R. Du, V. Nosenko, and H. Löwen, Statistical mechanics where Newton's third law is broken, Phys. Rev. X **5**, 011035 (2015).

[51] K. Yosioka and Y. Kawasima, Acoustic radiation pressure on a compressible sphere, Acta Acust. Acust. **5**, 167 (1955).
[52] G. T. Silva, An expression for the radiation force exerted by an acoustic beam with arbitrary wavefront (L), J. Acoust. Soc. Am. **130**, 3541 (2011).
[53] A. A. Doinikov, Acoustic radiation pressure on a rigid sphere in a viscous fluid, Proc. R. Soc. Lond. A **447**, 447 (1994).
[54] O. A. Sapozhnikov and M. R. Bailey, Radiation force of an arbitrary acoustic beam on an elastic sphere in a fluid, J. Acoust. Soc. Am. **133**, 661 (2013).
[55] P. J. Westervelt, The theory of steady forces caused by sound waves, J. Acoust. Soc. Am. **23**, 312 (1951).
[56] X. Zheng and R. E. Apfel, Acoustic interaction forces between two fluid spheres in an acoustic field, J. Acoust. Soc. Am. **97**, 2218 (1995).
[57] A. A. Doinikov, Acoustic radiation interparticle forces in a compressible fluid, J. Fluid Mech. **444**, 1 (2001).
[58] P. Gabrielli and M. Mercier-Finidori, Acoustic scattering by two spheres: Multiple scattering and symmetry considerations, J. Sound Vib. **241**, 423 (2001).
[59] A. R. Edmonds, *Angular Momentum in Quantum Mechanics* (Princeton University, Princeton, 1996), pp. 45–52.
[60] V. Bjerknes, *Fields of Force* (Columbia University, New York, 1906).
[61] A. Garcia-Sabaté, A. Castro, M. Hoyos, and R. González-Cinca, Experimental study on inter-particle acoustic forces, J. Acoust. Soc. Am. **135**, 1056 (2014).
[62] M. Settnes and H. Bruus, Forces acting on a small particle in an acoustical field in a viscous fluid, Phys. Rev. E **85**, 016327 (2012).
[63] P. C. Chaumet and M. Nieto-Vesperinas, Time-averaged total force on a dipolar sphere in an electromagnetic field, Opt. Lett. **25**, 1065 (2000).
[64] J. Happel and H. Brenner, *Low Reynolds Number Hydrodynamics* (Springer, New York, 2012).